Archives of Materials Science and Engineering
Volume 121
Issue 2
June 2023
Pages 71-79
International Scientific Journal
published monthly by the
World Academy of Materials
and Manufacturing Engineering

DOI: 10.5604/01.3001.0053.8488

Numerical modelling of planned corner deposition in 3D concrete printing

K. El Abbaoui [a,*], I. Al Korachi [a], M.T. Mollah [b], J. Spangenberg [b]

[a] Euromed Polytechnic School, Euromed Research Center, Euromed University of Fez, Route de Meknès (Rond-point Bensouda), 30000 Fès, Morocco

[b] Department of Civil and Mechanical Engineering, Technical University of Denmark, 2800 Kgs. Lyngby, Denmark

* Corresponding e-mail address: k.elabbaoui@ueuromed.org

ORCID identifier: https://orcid.org/0000-0002-5007-7714 (K.E.A.)

ABSTRACT

Purpose: Analysis of different path planning strategies and the effects of changing printhead direction in the geometrical conformity and the process precision around 90° corner in order to enable a simple and cost-effective way of facilitating the determination of an optimal printing mode for fast and accurate print corners in 3D concrete printing.

Design/methodology/approach: The material flow is characterized by a viscoplastic Bingham fluid. The printhead moves according to a prescribed speed to print the trajectory. The model solves the Navier-Stokes equations and uses the volume of fluid (VOF) technique. The acceleration steps and jerk (j) carry out the direction change. A smoothing factor is provided to smooth the toolpath. Several simulations were performed by varying the smoothing factor and jerk.

Findings: Overfilling at the sharp corner was found when the printhead velocity was kept constant while extruding mortar at a fixed extrusion velocity; however, proportional extrusion velocity with the printhead motion has improved the quality of the corner. Otherwise, a slight improvement in the corner shape related to applying a jerk was found.

Research limitations/implications: The Computational Fluid Dynamics (CFD) model could take an important amount of computing time to solve the problem; however, it serves as an efficient tool for accelerating different costly and time-consuming path planning processes for 3D concrete printing. Smaller angles and tilted printhead positions should be numerically and experimentally investigated in future research.

Practical implications: The developed CFD model is suited for executing parametric studies in parallel to determine the appropriate printing motion strategy for each trajectory with corners.

Originality/value: Computational Fluid Dynamics investigation of the path planning strategy for printing trajectory with a right-angle corner in 3D concrete printing.

Keywords: 3D concrete printing, CFD modelling, Path-planning, Corner precision, Mortar extrusion

Reference to this paper should be given in the following way:

K. El Abbaoui, I. Al Korachi, M.T. Mollah, J. Spangenberg, Numerical modelling of planned corner deposition in 3D concrete printing, Archives of Materials Science and Engineering 121/2 (2023) 71-79. DOI: https://doi.org/10.5604/01.3001.0053.8488

METHODOLOGY OF RESEARCH, ANALYSIS AND MODELLING

1. Introduction

As an additive manufacturing process [1], 3D concrete printing (3DCP) has gained significant attention over recent years due to its ability for structural customization and printing scale. This process consists of depositing successive layers of concrete contouring an object without formwork, i.e., by direct concrete placement. Therefore, 3DCP is a free-form buildup [2] and was proved in rationalising ecological materials [3,4]. The basic physics of the full of manufacturing steps of 3DCP was detailed in the reference [5]. These steps require special characteristics of a fresh mortar mixture to conform to the sophisticated needs of the real 3DCP experiment program. Particularly, a printable fresh mortar should be able to flow easily through the pump until the nozzle orifice and be flowable at the extrusion-deposition phase (i.e., retain its self-weight and that of the next layers without deforming as much as possible) [6]. These special characteristics depend on the printing open time, which in turn depends on the mixed design of the fresh mortar. Apart from design and optimization in robotic machines, one of the crucial challenges for a valid 3DCP experiment is the formulation of printable fresh mixtures. These materials are designed to be layered without collapse or shrinkage [7].

Despite its enormous progress, the process is still accompanied by several errors and failures. Concretes and mortars are usually Portland cement-based, leading to carbon dioxide emissions [8,9]. A specific constraint is that an angular toolpath needs to be implemented at the corner, which is typically rounded. The trajectory planner sits between the G-code and the servomotor execution of the toolpath travel. The G-code file may contain a million lines in it because of how much path error is permissible, how long it is going to take, how smoothly desired, the axes coupled and dynamic computation. Printing objects come with an understanding of the extruder dynamics of the 3D printer and how to plan the path [10]. Fleck et al. [11] observed an overflow at the corner because of trapezoidal velocity profiles employed through Marlin firmware [12]. This firmware involves a slam velocity at the turn. Research work has been done on material extrusion-based additive manufacturing investigating the print precision of cornering [13,14]. Giberti et al. [15] proposed an algorithm for path planning to inspect the material extrusion rate strained by velocity pursuant to a toolpath over the execution of the 3D printing process. Jin et al. [16] tried to smooth paths by decreasing the number of sharp corners using an implicit algorithm. Bos et al. [17] mentioned that square nozzles should be tangent to the toolpath when moving the printhead to overcome the twisting of the filament. AlSakka et al. [18] identified the optimal deposition path of the 3DCP, which reduces the weak bonds and preserves the buildability of the extruded material by using a discrete event model.

In complement to the physical printing, CFD modelling is able to reproduce the extrusion-deposition of the printable concrete and investigate some specific constraints to the physical print [19-22]. The angular toolpath planning in 3DCP is in its infancy. However, several CFD modelling studies have been performed in other 3D printing technologies, like fused deposition modelling. [23,24] developed CFD models to investigate the underfill and overflow areas in the deposited corners and investigated to smoothen the corners. Furthermore, Mollah et al. [25] investigated corner deposition for Bowden and Direct-drive extruders, where the Direct-drive extruder controls the amount of material extrusion near the corner. These models were developed using the Newtonian fluid model. In the present study, a CFD model is developed to solve the Navier-Stokes equations with the Bingham rheological model to simulate the mortar extrusion through a cylindrical nozzle. The simulations predict the evolution of the layer shape and the overfill area of a deposited mortar at a turn of 90° angle. Different printing ways are simulated to inquire about the consequences of smoothing the extruder nozzle with a constant extrusion rate. The structure of the study is as follows. Section 2 describes the methodology of the study with the theoretical details, CFD model, and path planning strategy. The results are discussed in section 3. Section 4 concludes the study.

2. Methodology

2.1. Governing equations

The flow dynamics of fresh mortar are modelled by the Navier Stokes equations for the non-Newtonian incompressible fluid with a constant density, formed by the following continuity (1) and the momentum equations (2):

$$\nabla \cdot \boldsymbol{u} = 0 \tag{1}$$

$$\rho\left(\frac{\partial \mathbf{u}}{\partial t}+\mathbf{u}\cdot\nabla\mathbf{u}\right)=-\nabla p+\rho\mathbf{g}+\nabla\cdot\boldsymbol{\sigma} \tag{2}$$

Where $\boldsymbol{u}$ is the velocity vector field, $\rho = 2100$ kg/m^3 is the density, p is the pressure, $\boldsymbol{g}$ is the gravitational vector field acting downwards, $\boldsymbol{\sigma}$ is the constitutive stress tensor, and t is the time variable. The rheology of the fresh mortar can be modelled by the viscoplastic Bingham model [26].

This type of fluid flows when the shear stress exceeds the yield stress. The evolution of the constitutive stress tensor can be approximated with the Generalized Newtonian Fluid constitutive model:

$$\boldsymbol{\sigma} = 2\eta_{app}(\dot{\gamma})\mathbf{D} \quad (3)$$

Where $\boldsymbol{D} = (\nabla \boldsymbol{u} + \nabla^T \boldsymbol{u})/2$ is the strain rate tensor, $\dot{\gamma} = (2tr(\boldsymbol{D}))^{1/2}$ is the shear rate, and $\eta_{app}(\dot{\gamma})$ is the apparent viscosity of the viscoplastic Bingham model. However, the apparent viscosity of the material increases to infinity when the applied stress is below the yield stress. To overcome this singularity issue of the Bingham fluid flow in the numerical simulation, the apparent viscosity is smoothed with the bi-viscosity method:

$$\eta_{app}(\dot{\gamma}) = \begin{cases} \eta_{MAX} & \text{for } \dot{\gamma} < \dot{\gamma}_c \\ \frac{\tau_Y}{\dot{\gamma}} + \mu_p & \text{for } \dot{\gamma} \geq \dot{\gamma}_c \end{cases} \quad (4)$$

Where $\tau_Y = 630$ Pa is the yield stress, $\mu_p = 7.5$ Pa.s is the plastic viscosity, $\eta_{MAX} = \tau_Y/\dot{\gamma}_c + \mu_p$ is the maximum value of the smoothed apparent viscosity and $\dot{\gamma}_c = 0.01$ s^{-1} is the critical threshold of the shear rate [19]. For more details on the regularization methods of the Bingham constitutive equation, please see [27].

2.2. CFD model

The physical problem was numerically simulated with the software FLOW-3D®, version 12.0 [28]. The equations (1) and (2) are discretized by the finite volume method. The volume of the fluid method [29] was used to capture the extrudate mortar sharp interfaces with the split Lagrangian method. The numerical domain (Fig. 1) was discretized with a uniform Cartesian non-conforming mesh. The cell size is 1 mm for each direction. A no-slip boundary condition was applied to the nozzle wall and the build plate. The fresh mortar begins to flow through the extruder nozzle with a constant velocity and exits with a fully developed flow profile. The other domain boundaries are set as continuative boundary conditions. The geometry of the model consists of a cylindrical nozzle and a build plate. The nozzle comes with an inner diameter of D = 25 mm and a thickness of e = 2 mm; the numerical domain occupies a volume of 240 x 230 x 65 mm^3. The distance between the nozzle outlet and the build space is fixed at h = 12.5 mm. The printhead starts to move with a prescribed velocity when the mortar reaches the build plate.

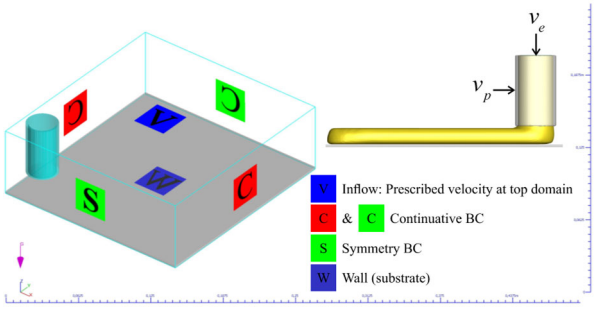

Fig. 1. CFD model

2.3. Path planning strategies

The path planning of deposited corners consists of printing two segments with a 90° turn without stopping the printhead (Fig. 2). The servomotor of the 3D printer controls the displacement through a finite jerk (j) and a linear acceleration limit. The jerk is the velocity leap that occurs instantly when the printhead begins an acceleration or a deceleration. Six depositing strategies of mortar layer with sharp and smooth corners have been simulated (Fig. 3). The printhead moves with a maximum velocity $v_p = 50$ mm/s, decelerates and accelerates at the corner with a maximum value $a = (30, 50)$ mm/s^2. The extrusion velocity $v_e = 33.4$ mm/s is kept constant along the path except in case 3, which is linearly proportional to the printing velocity along X-Y axes ($v_e \propto v_p$). Case 0 presents the most used printing strategy in 3DCP, where the jerk is infinite because of the very short servo time at the acceleration transitions (transition time of 0.0001 s). A smoothing factor $\varsigma_m = \delta/T$ was used to smooth the printhead trajectory around the corner. δ and T denote the acceleration time limit and the deceleration phase time required to decrease the velocity of the printhead until it stops in the first direction (X-axis in our cases), respectively. Table 1 presents the path-planning strategies that are numerically simulated.

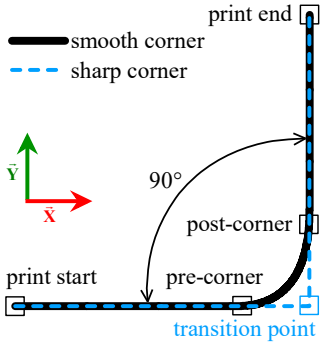

Fig. 2. Smoothed trajectory at a 90° turn

Table 1.
Path planning strategies cases numerically simulated

Corner type	Case ID	Smoothing factor ς_m
Sharp corner	0	0 (j = ∞)
	1	0 (j = 0)
	2	0 (j = 20 mm/s)
	3	0 (j = 20 mm/s; $v_e \propto v_p$)
Smooth corner	4	0.3
	5	1.0

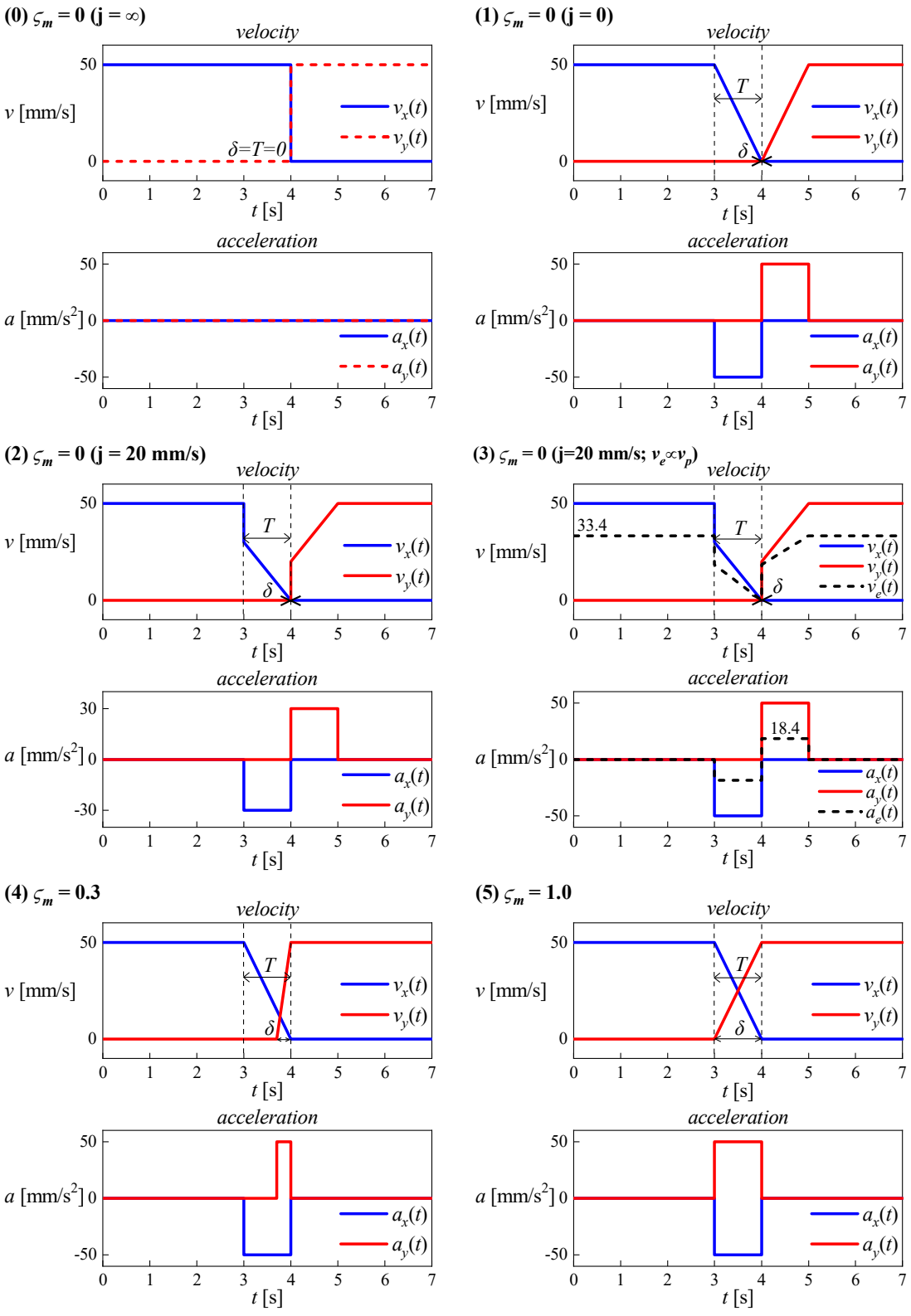

Fig. 3. Velocity and acceleration profiles in the X-Y directions for 90° turn according to the six printing strategies

3. Results and discussion

The simulated results of the deposition flow are post-processed using FlowSight, version 12.0 and presented in Figure 4. In the left side of the figure; we illustrate a perspective view of the different simulated strategies. The right side shows the ideal widths and the maximum flow depth of the different deposited layers.

To exactly execute a toolpath with the G-code of the 3D printer, the extruder nozzle has to stop every time reaching a corner because, in each segment of the toolpath, the extruder nozzle moves at a fixed ratio between the motors. When coming to a stop at the corner, the flow rate drew from the extruder nozzle, and it will take a long time to deposit. Figures 4a, 4b and 4c correspond to the sharp corner cases with constant v_e. The first strategy corresponds to an ideal model with an infinite jerk where we have to be aware because it could cause vibration and slam to the printhead, and as a result, a poor deposition could be obtained. It is observed that the selected jerk slightly improves the print quality of the corner (Fig. 4c). Furthermore, the mortar overflowed and crushed at the 90° turn. This is occurring because of the feed rate that has been kept constant and the increase of the extrusion pressure due to the slowing of the printhead while changing direction.

In order to smooth corners, it is needed to act on the velocity, acceleration and jerk limits of the actuator of the 3D printer. Figure 4e shows an overflow at the exterior of the turn due to the corner shape and the acceleration time limit of 0.3 s.

The accuracy print is obtained when the acceleration and the deceleration steps are blended instantly. Figure 4f shows a uniform corner bounded by an elliptical arc through the endpoints with a minimal overflow at the exterior of the turn despite the smoothing of the toolpath. The observation is that when the nozzle goes through the corner, the velocity is momentarily decelerated and accelerated. Therefore, a curvilinear path at the corner exterior is obtained.

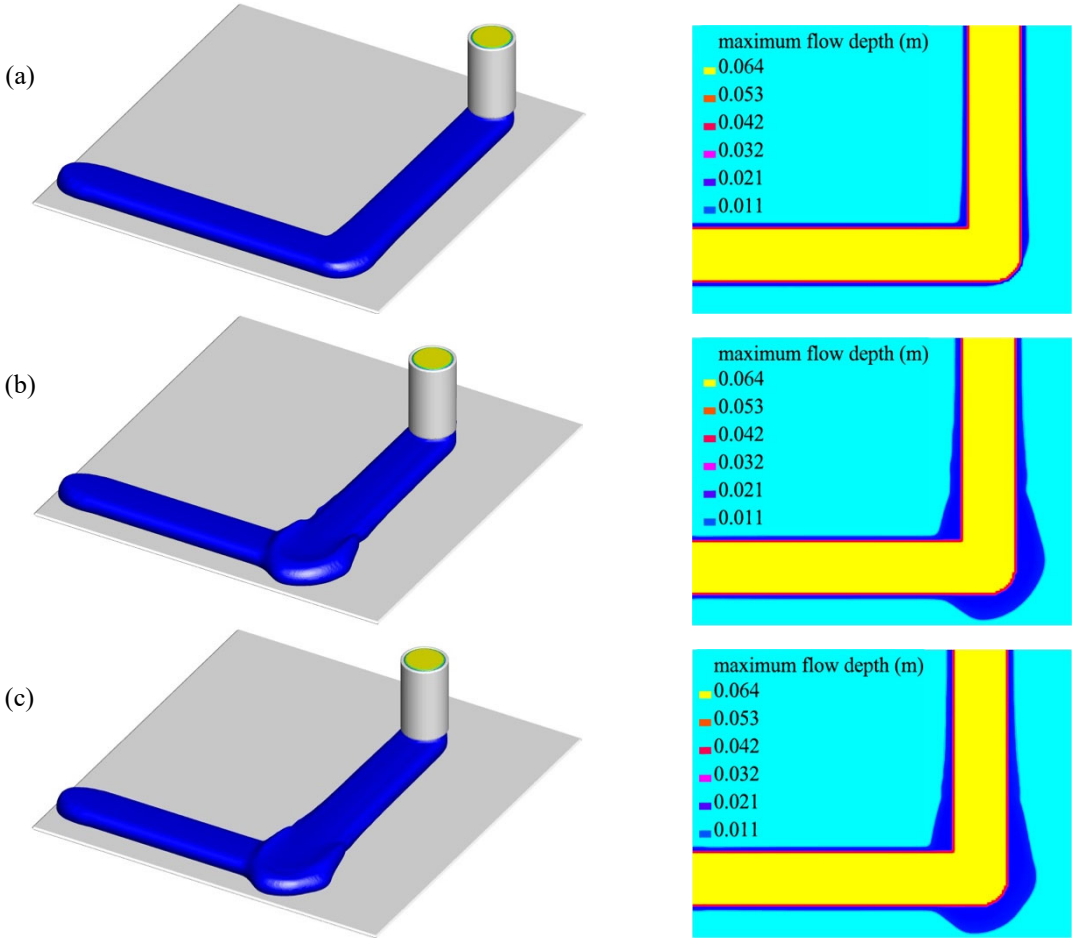

Fig. 4. a)-c) Simulations of six deposition strategies of mortar extrusion along a 90° turn angle

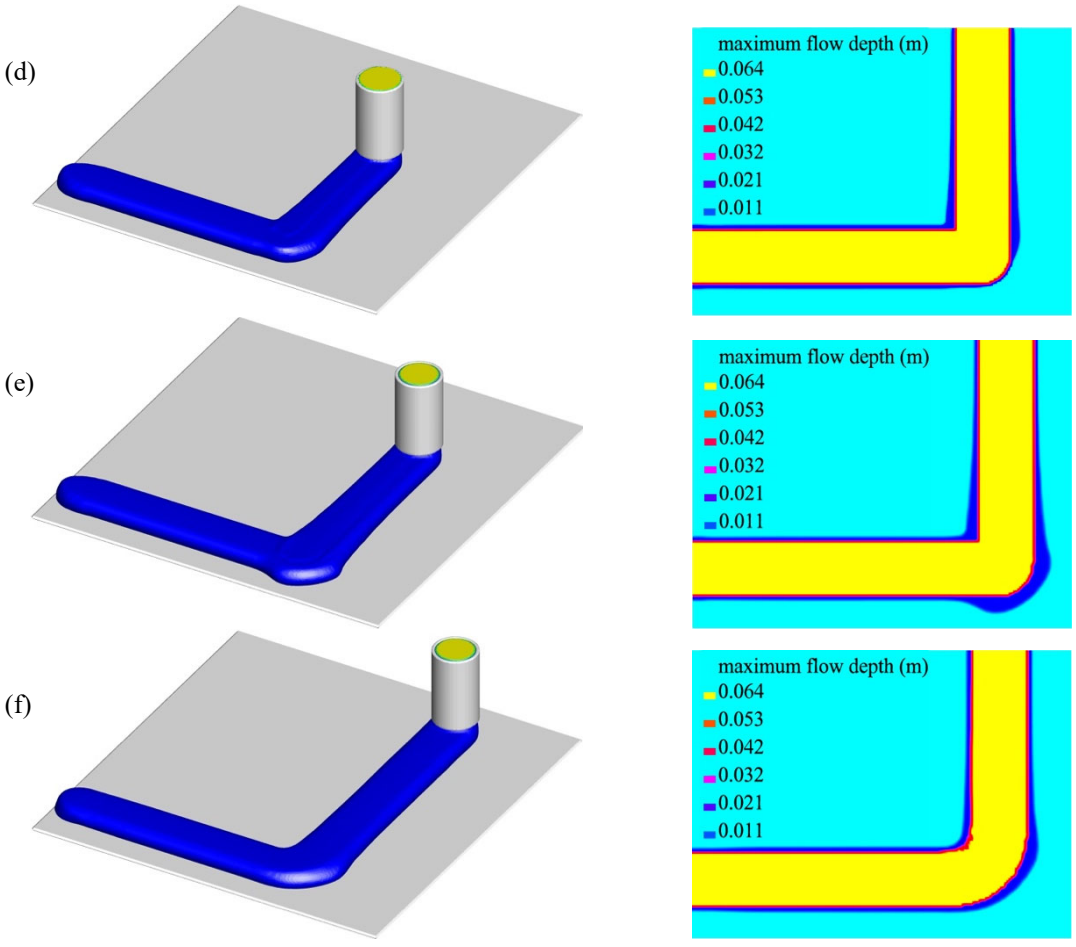

Fig. 4. d)-f) Simulations of six deposition strategies of mortar extrusion along a 90° turn angle

Figure 5 shows the variant of the trajectory length for the six printing strategies obtained by summation of the elementary lengths travelled during the time interval [0, 7s]. The trajectory length decreases largely with respect to the linear curve (the ideal print, which represents the maximum achieved length, case 0) when the corner is not smoothed (cases 1, 2 and 3). However, the trajectory length decreases slightly from the linear curve when the corner is smoothed (cases 4 and 5). It's worth noting that the distance travelled by the printhead describes a non-uniform motion at the turn for the sharp corner strategies because it increases non-linearly with time.

In order to print corners, the distance travelled by the printhead should be taken into account in the path planning strategy to achieve a shorter trajectory length. A shorter trajectory length means that the printhead has to travel a shorter distance by determining the optimal path, taking into account the capabilities of the 3D printer, which can reduce the printing time and the amount of material used, leading to an efficient and reliable 3DCP process.

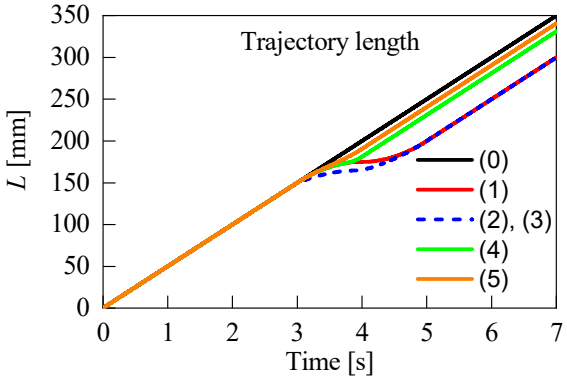

Fig. 5. Trajectory length of the six deposition strategies

The overflow and the underflow amount at the inside and the outside of the corner with a 90° angle for the studied printing strategies (cases 1, 2, 3, 4 and 5) regarding the ideal print (case 0) were quantified to analyze the deposition behaviour when the printhead initiate a turn (Fig. 6).

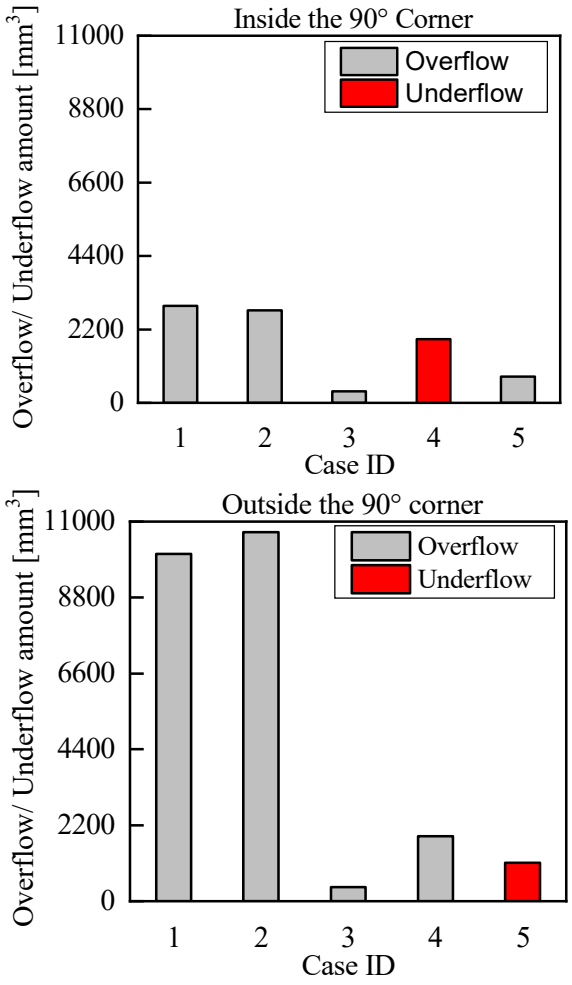

Fig. 6. Underflow/Overflow amount at the inside and the outside of the 90° corner

The red bars quantify the lack of material at the corner zone according to the ideal print. The virtual printed layer for the sharp corner strategy applying a jerk of 20 mm/s was noticeably improved because of the synchronization of the extrusion rate at the direction change of the printhead. As illustrated on the graphs, the deposited material largely overflowed at the exterior side of the turn compared to the interior side for all the toolpath planning scenarios. This is because the double deposition occurs at the inner side of the turn, one from the pre-corner layer and the other from the post-corner layer. In addition, the toolpath of the printhead was fitted at the turn to have a curvature line without reaching the sharp corner. Therefore, the precision of the print quality depends on the way we program the print settings of the 3D printer machine, the designed fresh mortar mixture, the followability characteristic, and its setting behaviour during and after the extrusion-deposition process.

4. Conclusions

A CFD model was developed to investigate different toolpath strategies to assess the corner precision in 3DCP. The rheology of the printable mortar is approximated with the Generalized Newtonian constitutive model using the Bingham rheological fluid model. A 90° turn was investigated.

- It was found that the printhead should be planned to not slam or slow to a stop for good print quality of corners.
- It was observed that the tested case involving a jerk of 20 mm/s and an extrusion rate synchronized with the nozzle speed reduces the swelling of the layer at the corner.
- A commensurate extrusion rate with the printing velocity should generate a uniform corner in the case of the 90° turn; however, it could create a major swelling of the layer in the case of smaller angles.

The present study shows that the CFD model could be used as a powerful tool to optimize the printing of different angular sharp turns in 3DCP experiments by selecting the appropriate printing strategy for each corner. This will minimize the number of prototypes and experimental tests required to implement toolpath strategies for corners with high precision. The experimental tests of 3D printing 90° corners in 3DCP were left for future research. The rheological behaviour of fresh mortar mixtures could be characterized by other constitutive equations, such as the Herschel-Bulkley model. Different nozzle geometry (e.g., square nozzle) and complex toolpath with small turn angles should be investigated in future studies.

Acknowledgements

Simulation result courtesy of Flow Science, Inc., developer of the computational fluid dynamics (CFD) software FLOW-3D® (https://www.flow3d.com).

References

[1] A. El Magri, S. Vaudreuil, Optimizing the mechanical properties of 3D-printed PLA-graphene composite using response surface methodology, Archives of Materials Science and Engineering 112/1 (2021) 13-22. DOI: https://doi.org/10.5604/01.3001.0015.5928

[2] J. Pegna, Exploratory investigation of solid freeform construction, Automation in Construction 5/5 (1997) 427-437. DOI: https://doi.org/10.1016/S0926-5805(96)00166-5

[3] G. De Schutter, K. Lesage, V. Mechtcherine, V.N. Nerella, G. Habert, I. Agusti-Juan, Vision of 3D printing with concrete - Technical, economic and environmental potentials. Cement and Concrete Research 112 (2018) 25-36. DOI: https://doi.org/10.1016/j.cemconres.2018.06.001

[4] M. Dixit, 3-D printing in building construction: a literature review of opportunities and challenges of reducing life cycle energy and carbon of buildings. In: IOP Conference Series: Earth and Environmental Science 290 (2019) 012012. DOI https://doi.org/10.1088/1755-1315/290/1/012012

[5] V. Mechtcherine, F.P. Bos, A. Perrot, W.L. da Silva, V. Nerella, S. Fataei, R.J. Wolfs, M. Sonebi, N. Roussel, Extrusion-based additive manufacturing with cement-based materials - Production steps, processes, and their underlying physics: A review, Cement and Concrete Research 132 (2020) 106037. DOI: https://doi.org/10.1016/j.cemconres.2020.106037

[6] R. Comminal, W.R.L. da Silva, T.J. Andersen, H. Stang, J. Spangenberg, Influence of processing parameters on the layer geometry in 3D concrete printing: experiments and modelling, in: F. Bos, S. Lucas, R. Wolfs, T. Salet (eds), Second RILEM International Conference on Concrete and Digital Fabrication. DC 2020, RILEM Bookseries, vol 28, Springer, Cham, 2020, 852-862. DOI: https://doi.org/10.1007/978-3-030-49916-7_83

[7] L. Prasittisopin, P. Jiramarootapong, K. Pongpaisanseree, C. Snguanyat, Lean manufacturing and thermal enhancement of single-layer wall with an additive manufacturing (AM) structure, ZKG International 4 (2019) 64-74.

[8] I. Nasser, M. Ali, M. Kadhim, Mechanical properties and microstructure of alkali activated mortar containing unexpanded clay, Archives of Materials Science and Engineering 113/2 (2022) 56-68. DOI: https://doi.org/10.5604/01.3001.0015.7018

[9] W. Tuvayanond, L. Prasittisopin, Design for Manufacture and Assembly of Digital Fabrication and Additive Manufacturing in Construction: A Review, Buildings 13/2 (2023) 429. DOI: https://doi.org/10.3390/buildings13020429

[10] J. Go, S.N. Schiffres, A.G. Stevens, A.J. Hart, Rate limits of additive manufacturing by fused filament fabrication and guidelines for high-throughput system design, Additive Manufacturing 16 (2017) 1-11. DOI: https://doi.org/10.1016/j.addma.2017.03.007

[11] T.J. Fleck, J.C. McCaw, S.F. Son, I.E. Gunduz, J.F. Rhoads, Characterizing the vibration-assisted printing of high viscosity clay material, Additive Manufacturing 47 (2021) 102256. DOI: https://doi.org/10.1016/j.addma.2021.102256

[12] Marlin-Firmware. Available form: https://marlinfw.org/meta/gcode/ (access in: 6.10.2022)

[13] B. Akhoundi, M. Nabipour, O. Kordi, F. Hajami, Calculating printing speed in order to correctly print PLA/continuous glass fiber composites via fused filament fabrication 3D printer. Journal of Thermoplastic Composite Materials 36/1 (2023) 162-181. DOI: https://doi.org/10.1177/0892705721997534

[14] L. Li, R. McGuan, R. Isaac, P. Kavehpour, R. Candler, Improving precision of material extrusion 3D printing by in-situ monitoring and predicting 3D geometric deviation using conditional adversarial networks, Additive Manufacturing 38 (2021) 101695. DOI: https://doi.org/10.1016/j.addma.2020.101695

[15] H. Giberti, L. Sbaglia, M. Urgo, A path planning algorithm for industrial processes under velocity constraints with an application to additive manufacturing, Journal of Manufacturing Systems 43/1 (2017) 160-167. DOI: https://doi.org/10.1016/j.jmsy.2017.03.003

[16] Y. Jin, J. Du, Z. Ma, A. Liu, Y. He, An optimization approach for path planning of high-quality and uniform additive manufacturing, The International Journal of Advanced Manufacturing Technology 92/1 (2017) 651-662. DOI: https://doi.org/10.1007/s00170-017-0207-3

[17] F. Bos, R. Wolfs, Z. Ahmed, T. Salet, Additive manufacturing of concrete in construction: potentials and challenges of 3D concrete printing, Virtual and Physical Prototyping 11/3 (2016) 209-225. DOI: https://doi.org/10.1080/17452759.2016.1209867

[18] F. AlSakka, M.H. Senan, A. Abou Yassin, F. Hamzeh, Path Optimization in 3D Concrete Printing to Minimize Weak Bonds Formation. Periodica Polytechnica Architecture 50/2 (2019) 163-168. DOI: https://doi.org/10.3311/PPar.12722

[19] R. Comminal, W.R.L. da Silva, T.J. Andersen, H. Stang, J. Spangenberg, Modelling of 3D concrete printing based on computational fluid dynamics. Cement and Concrete Research 138 (2020) 106256. DOI: https://doi.org/10.1016/j.cemconres.2020.106256

[20] N. Roussel, J. Spangenberg, J. Wallevik, R. Wolfs, Numerical simulations of concrete processing: From standard formative casting to additive manufacturing, Cement and Concrete Research 135 (2020) 106075. DOI: https://doi.org/10.1016/j.cemconres.2020.106075

[21] J. Spangenberg, W.R.L. da Silva, R. Comminal, M.T. Mollah, T.J. Andersen, H. Stang, Numerical simulation of multi-layer 3D concrete printing. RILEM Technical Letters 6 (2021) 119-123. DOI: https://doi.org/10.21809/rilemtechlett.2021.142

[22] J. Spangenberg, W.R.L. da Silva, M.T. Mollah, R. Comminal, T.J. Andersen, H. Stang, Integrating Reinforcement with 3D Concrete Printing: Experiments and Numerical Modelling, in: R. Buswell, A. Blanco, S. Cavalaro, P. Kinnell (eds), Third RILEM International Conference on Concrete and Digital Fabrication, DC 2022, RILEM Bookseries, vol 37, Springer, Cham, 2022, 379-384. DOI: https://doi.org/10.1007/978-3-031-06116-5_56

[23] R. Comminal, M.P. Serdeczny, D.B. Pedersen, J. Spangenberg, Numerical modeling of the material deposition and contouring precision in fused deposition modelling, Proceedings of the 29th Annual International Solid Freeform Fabrication Symposium, Austin, TX, USA, 2018, 13-15.

[24] R. Comminal, M.P. Serdeczny, D.B. Pedersen, J. Spangenberg, Motion planning and numerical simulation of material deposition at corners in extrusion additive manufacturing, Additive Manufacturing 29 (2019) 100753. DOI: https://doi.org/10.1016/j.addma.2019.06.005

[25] M.T. Mollah, A. Moetazedian, A. Gleadall, J. Yan, W.E. Alphonso, R.B. Comminal, B. Seta, T. Lock, J. Spangenberg, Investigation on corner precision at different corner angles in material extrusion additive manufacturing: An experimental and computational fluid dynamics analysis, Proceedings of the 33rd Annual International Solid Freeform Fabrication Symposium, Austin, TX, USA, 2022, 872-881.

[26] N. Roussel, Rheological requirements for printable concretes, Cement and Concrete Research 112 (2018) 76-85. DOI: https://doi.org/10.1016/j.cemconres.2018.04.005

[27] Y. Tu, A. Hassan, A. Siadat, G. Yang, Z. Chen, Numerical simulation and experimental validation of deposited corners of any angle in direct ink writing, The International Journal of Advanced Manufacturing Technology 123 (2022) 559-570. DOI: https://doi.org/10.1007/s00170-022-10195-2

[28] Flow Science, Inc. FLOW-3D, Version 12.0, Santa Fe, NM, 2019.

[29] C.W. Hirt, B.D. Nichols, Volume of fluid (VOF) method for the dynamics of free boundaries, Journal of Computational Physics 39/1 (1981) 201-225. DOI: https://doi.org/10.1016/0021-9991(81)90145-5